Geometry of the effective Majorana neutrino mass in the $0\nu\beta\beta$ decay *

XING Zhi-zhong(邢志忠)[1,2;1)] ZHOU Ye-Ling(周也铃)[1;2)]

[1] Institute of High Energy Physics, Chinese Academy of Sciences, P.O. Box 918, Beijing 100049, China
[2] Center for High Energy Physics, Peking University, Beijing 100080, China

Abstract: The neutrinoless double-beta ($0\nu\beta\beta$) decay is a unique process used to identify the Majorana nature of massive neutrinos, and its rate depends on the size of the effective Majorana neutrino mass $\langle m\rangle_{ee}$. We put forward a novel 'coupling-rod' diagram to describe $\langle m\rangle_{ee}$ in the complex plane, by which the effects of the neutrino mass ordering and CP-violating phases on $\langle m\rangle_{ee}$ are intuitively understood. We show that this geometric language allows us to easily obtain the maximum and minimum of $|\langle m\rangle_{ee}|$. It remains usable even if there is a kind of new physics contributing to $\langle m\rangle_{ee}$, and it can also be extended to describe the effective Majorana masses $\langle m\rangle_{e\mu}$, $\langle m\rangle_{e\tau}$, $\langle m\rangle_{\mu\mu}$, $\langle m\rangle_{\mu\tau}$ and $\langle m\rangle_{\tau\tau}$ which may appear in some other lepton-number violating processes.

Key words: Majorana particles, neutrino mass, $0\nu\beta\beta$ decay

PACS: 14.60.Pq, 13.15.+g, 25.30.Pt **DOI:** 10.1088/1674-1137/39/1/011001

1 Introduction

Whether massive neutrinos are Majorana particles remains an open question in particle physics. By definition, a Majorana neutrino is its own antiparticle [1], and this consequently leads to lepton number violation. Because the masses of three known neutrinos are extremely small, the only feasible way to identify their Majorana nature is to detect the neutrinoless double-beta ($0\nu\beta\beta$) decay of some even-even nuclei [2]: $N(A,Z)\to N(A,Z+2)+2e^-$, in which the lepton number is violated by two units. On the basis where flavor and mass eigenstates of the charged leptons coincide with each other, the $0\nu\beta\beta$ decay rate is controlled by the (e,e) element of the effective Majorana neutrino mass matrix [3]

$$M_\nu = \begin{pmatrix} \langle m\rangle_{ee} & \langle m\rangle_{e\mu} & \langle m\rangle_{e\tau} \\ \langle m\rangle_{\mu e} & \langle m\rangle_{\mu\mu} & \langle m\rangle_{\mu\tau} \\ \langle m\rangle_{\tau e} & \langle m\rangle_{\tau\mu} & \langle m\rangle_{\tau\tau} \end{pmatrix},$$

$$\langle m\rangle_{\alpha\beta} \equiv \sum_i \left(m_i U_{\alpha i} U_{\beta i}\right), \tag{1}$$

where the Greek subscripts run over e, μ and τ, m_i denotes the i-th neutrino mass, and $U_{\alpha i}$ stands for the corresponding element of the lepton flavor mixing matrix U [4]. Of course, $\langle m\rangle_{\alpha\beta}=\langle m\rangle_{\beta\alpha}$ holds for symmetric M_ν. In the standard three-flavor scheme, U is a unitary matrix and can therefore be parametrized in terms of three flavor mixing angles and three CP-violating phases:

$$U=\begin{pmatrix} c_{12}c_{13} & s_{12}c_{13} & s_{13}e^{-i\delta} \\ -s_{12}c_{23}-c_{12}s_{13}s_{23}e^{i\delta} & c_{12}c_{23}-s_{12}s_{13}s_{23}e^{i\delta} & c_{13}s_{23} \\ s_{12}s_{23}-c_{12}s_{13}c_{23}e^{i\delta} & -c_{12}s_{23}-s_{12}s_{13}c_{23}e^{i\delta} & c_{13}c_{23} \end{pmatrix} P_\nu, \tag{2}$$

where $c_{ij}\equiv\cos\theta_{ij}$, $s_{ij}\equiv\sin\theta_{ij}$ (for ij=12, 13, 23), and $P_\nu=\mathrm{Diag}\{e^{i\rho/2},1,e^{i(\delta+\sigma/2)}\}$. As a result, the effective mass term of the $0\nu\beta\beta$ decay reads

$$\begin{aligned}\langle m\rangle_{ee} &= m_1|U_{e1}|^2e^{i\rho}+m_2|U_{e2}|^2+m_3|U_{e3}|^2e^{i\sigma} \\ &= m_1c_{12}^2c_{13}^2e^{i\rho}+m_2s_{12}^2c_{13}^2+m_3s_{13}^2e^{i\sigma}.\end{aligned} \tag{3}$$

So far the values of θ_{12}, θ_{13} and θ_{23} have been determined to a good degree of accuracy from current neutrino oscillation data, but the three phase parameters remain unknown [5]. While the value of $\Delta m^2_{21}\equiv m_2^2-m_1^2$ and the absolute value of $\Delta m^2_{31}\equiv m_3^2-m_1^2$ are also measured, the sign of Δm^2_{31} and the absolute neutrino mass scale

Received 3 June 2014
∗ Supported by National Natural Science Foundation of China (11135009)
1) E-mail: xingzz@ihep.ac.cn
2) E-mail: zhouyeling@ihep.ac.cn

remain unknown. Hence the size of $\langle m\rangle_{\rm ee}$ suffers from three kinds of uncertainty even without any new physics pollution:

(1) The unknown absolute neutrino mass scale (i.e. the value of m_1, m_2 or m_3);

(2) The unknown neutrino mass ordering (i.e. either $\Delta m^2_{31}>0$ or $\Delta m^2_{31}<0$);

(3) The unknown Majorana CP-violating phases ρ and σ appearing in $|\langle m\rangle_{\rm ee}|$.

Up to now, a lot of phenomenological efforts have been made to probe the parameter space of $\langle m\rangle_{\rm ee}$ and discuss its sensitivity to possible new physics [6].

In the present work we are going to put forward a novel 'coupling-rod' diagram to describe the salient features of $\langle m\rangle_{\rm ee}$ in the complex plane, by which the effects of the neutrino mass ordering and CP-violating phases on $\langle m\rangle_{\rm ee}$ can be intuitively understood. Some special but interesting cases, including the behavior of $\langle m\rangle_{\rm ee}$ with $m_1=0$ or $m_3=0$ and the maximum or minimum of $|\langle m\rangle_{\rm ee}|$ in two different neutrino mass spectra, are easily explained in this geometric language. We point out that the coupling-rod diagram remains applicable even if a kind of new physics, such as an extra light but sterile neutrino, contributes to $\langle m\rangle_{\rm ee}$. It can also be extended to provide a vivid description of the effective Majorana neutrino masses $\langle m\rangle_{\rm e\mu}$, $\langle m\rangle_{\rm e\tau}$, $\langle m\rangle_{\rm \mu\mu}$, $\langle m\rangle_{\rm \mu\tau}$ and $\langle m\rangle_{\rm \tau\tau}$, which may show up in neutrino-antineutrino oscillations and some other lepton-number violating processes.

2 The coupling-rod diagram of $\langle m\rangle_{\rm ee}$

Given $\Delta m^2_{21}>0$ as established from the solar neutrino oscillation data, the unfixed sign of Δm^2_{31} implies that the neutrino mass ordering can be either normal (i.e. $m_1<m_2<m_3$) or inverted (i.e. $m_3<m_1<m_2$). In particular, the possibility of $m_1=0$ or $m_3=0$ is still allowed by current experimental data. Because of $m_2>0$, together with

$$\begin{aligned} m_1&=\sqrt{m_2^2-\Delta m^2_{21}},\\ m_3&=\sqrt{m_2^2-\Delta m^2_{21}+\Delta m^2_{31}}, \end{aligned} \tag{4}$$

we find that it is most convenient to take the nonzero $m_2U^2_{\rm e2}$ term as the base vector to geometrically describe $\langle m\rangle_{\rm ee}$ in the complex plane[1)]. Taking account of the phase convention of P_ν in Eq. (3), which allows $U_{\rm e2}$ to be real and positive, we have

$$\begin{aligned} \overrightarrow{OA}&\equiv m_2U^2_{\rm e2}=m_2|U_{\rm e2}|^2,\\ \overrightarrow{AB}&\equiv m_1U^2_{\rm e1}=m_1|U_{\rm e1}|^2{\rm e}^{{\rm i}\rho},\\ \overrightarrow{CO}&\equiv m_3U^2_{\rm e3}=m_3|U_{\rm e3}|^2{\rm e}^{{\rm i}\sigma}, \end{aligned} \tag{5}$$

as illustrated in Fig. 1. So the vector $\overrightarrow{CB}=\overrightarrow{OA}+\overrightarrow{AB}+\overrightarrow{CO}$, which connects the two circles formed by the rotations of $\overrightarrow{AB}$ and $\overrightarrow{OC}$ about their respective origins A and O, looks like the 'coupling rod' of a locomotive and stands for $\langle m\rangle_{\rm ee}$. Depending on the length of $\overrightarrow{OA}$ and the radii of $\odot O$ and $\odot A$, there are five possibilities for the relative positions of these two circles:

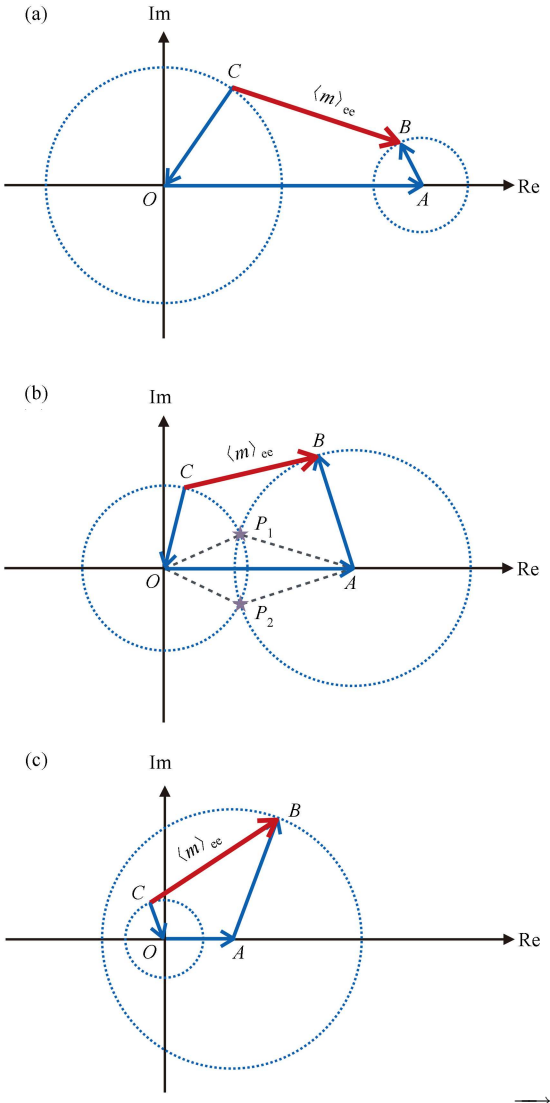

Fig. 1. The coupling-rod diagram of $\langle m\rangle_{\rm ee}\equiv\overrightarrow{CB}$ in the complex plane, where $\overrightarrow{OA}\equiv m_2|U_{\rm e2}|^2$, $\overrightarrow{AB}\equiv m_1|U_{\rm e1}|^2{\rm e}^{{\rm i}\rho}$ and $\overrightarrow{CO}\equiv m_3|U_{\rm e3}|^2{\rm e}^{{\rm i}\sigma}$. If the neutrino mass ordering is normal, the three configurations of $\langle m\rangle_{\rm ee}$ are all possible; but if the neutrino mass ordering is inverted, then only Fig. 1(c) is allowed.

(1) $AB+OC<OA$ as shown in Fig. 1(a), or equivalently $m_1\cos^2\theta_{12}+m_3\tan^2\theta_{13}<m_2\sin^2\theta_{12}$. Namely,

1) Some authors have chosen the $m_1U^2_{\rm e1}$ term as the base vector to illustrate the geometry of $\langle m\rangle_{\rm ee}$ [7]. Such a choice has a remarkable disadvantage, because the $m_1\to0$ limit will make this geometric language invalid.

$\odot O$ and $\odot A$ are external to each other, and thus $|\langle m\rangle_{\rm ee}| = BC > 0$ holds. The allowed range of $|\langle m\rangle_{\rm ee}|$ turns out to be $OA-AB-OC \leqslant |\langle m\rangle_{\rm ee}| \leqslant OA+AB+OC$.

(2) $AB+OC = OA$, or equivalently $m_1\cos^2\theta_{12} + m_3\tan^2\theta_{13} = m_2\sin^2\theta_{12}$. Namely, $\odot O$ and $\odot A$ touch externally on the horizontal axis. At the touching point $\rho=\sigma=\pi$ and $|\langle m\rangle_{\rm ee}|=BC=0$ hold. In this special case the quadrilateral collapses into lines, and thus m_2 can be uniquely determined in terms of Δm^2_{21}, Δm^2_{31}, θ_{12} and θ_{13}. We find $m_2 \approx 8.4$ MeV to 9.9 MeV by using the 3σ ranges of the four input parameters [8]. It will be explained later on that only the normal neutrino mass ordering is suitable for this case.

(3) $|AB-OC|<OA<AB+OC$ as shown in Fig. 1(b), where $\odot O$ and $\odot A$ intersect. The two points of intersection imply $|\langle m\rangle_{\rm ee}|=BC=0$; namely, the quadrilateral collapses into a triangle. In this case, however, the two Majorana phases should take some nontrivial values [9].

(4) $AB-OC = OA$, or equivalently $m_1\cos^2\theta_{12} - m_3\tan^2\theta_{13} = m_2\sin^2\theta_{12}$. Namely, $\odot O$ and $\odot A$ touch internally on the horizontal axis. At the touching point $\rho=\pi$ and $\sigma=0$ hold, so does $|\langle m\rangle_{\rm ee}|=BC=0$. In this special case we find $m_2 \approx 9.5$ MeV to 13.7 MeV by inputting the 3σ ranges of the four parameters [8]. Only the normal neutrino mass ordering is suitable for this case.

(5) $AB-OC > OA$ as shown in Fig. 1(c), where $\odot O$ and $\odot A$ do not touch and the former is contained in the latter. In this case $|\langle m\rangle_{\rm ee}| = BC > 0$ holds. The allowed arrangement of $|\langle m\rangle_{\rm ee}|$ turns out to be $AB-OA-OC \leqslant |\langle m\rangle_{\rm ee}| \leqslant AB+OA+OC$.

Note that the above discussions are not apparently subject to the neutrino mass ordering, but the situation will be remarkably simpler if the neutrino mass ordering is inverted. To see this point clearly, let us take into account $|\Delta m^2_{31}| \sim 30\Delta m^2_{21}$ and $|U_{\rm e1}|^2 \sim 2|U_{\rm e2}|^2 \sim 30|U_{\rm e3}|^2$ as indicated by current experimental data [8]. So $\Delta m^2_{31}<0$ leads us to $m_3<m_1\lesssim m_2$, and the relative length of OC becomes maximal when the three neutrino masses are nearly degenerate (i.e. $m_3 \lesssim m_1 \lesssim m_2$). In the latter case we are simply left with $AB{:}OA{:}OC \sim |U_{\rm e1}|^2{:}|U_{\rm e2}|^2{:}|U_{\rm e3}|^2 \sim 30{:}15{:}1$, and thus it is impossible to satisfy either $AB+OC \leqslant OA$ or $|AB-OC| \leqslant OA$. In other words, only $AB-OC>OA$ can be satisfied in the inverted neutrino mass ordering, and this observation stays valid no matter whether m_3 is vanishing or close to the value of m_1, or in between. We arrive at two conclusions about $\langle m\rangle_{\rm ee}$ in Fig. 1: (1) when $m_1<m_2<m_3$ holds, the possibilities illustrated in Fig. 1(a), (b) and (c) are all allowed, and they correspond to the values of m_1 which are small ($m_1 \ll m_2 \ll m_3$), medium and large ($m_1 \lesssim m_2 \lesssim m_3$), respectively; (2) when $m_3<m_1<m_2$ holds, only the possibility shown in Fig. 1(c) is allowed, excluding $|\langle m\rangle_{\rm ee}|=0$ in this case.

The geometric language has helped us to understand some salient features of $\langle m\rangle_{\rm ee}$. We proceed to discuss the maximum and minimum of $|\langle m\rangle_{\rm ee}|$ in an analytical way. Eq. (3) can be rewritten as

$$\begin{aligned}\langle m\rangle_{\rm ee} &= m_2|U_{\rm e2}|^2\left[1+\frac{m_1}{m_2}\frac{|U_{\rm e1}|^2}{|U_{\rm e2}|^2}{\rm e}^{{\rm i}\rho}+\frac{m_3}{m_2}\frac{|U_{\rm e3}|^2}{|U_{\rm e2}|^2}{\rm e}^{{\rm i}\sigma}\right]\\ &= m_2\sin^2\theta_{12}\cos^2\theta_{13}\left[1+\sqrt{1-\frac{\Delta m^2_{21}}{m^2_2}}\cot^2\theta_{12}{\rm e}^{{\rm i}\rho}\right.\\ &\quad\left.+\sqrt{1-\frac{\Delta m^2_{21}}{m^2_2}+\frac{\Delta m^2_{31}}{m^2_2}}\frac{\tan^2\theta_{13}}{\sin^2\theta_{12}}{\rm e}^{{\rm i}\sigma}\right],\end{aligned} \tag{6}$$

where $m_2 \geqslant \sqrt{\Delta m^2_{21}}$ must hold for the normal mass ordering, or $m_2 \geqslant \sqrt{\Delta m^2_{21}-\Delta m^2_{31}}$ must hold for the inverted mass ordering. With the help of the intuitive coupling-rod diagram of $\langle m\rangle_{\rm ee}$ in Fig. 1, we can obtain the maximum or minimum of $|\langle m\rangle_{\rm ee}|$ in two different cases:

(1) $m_1 < m_2 < m_3$. In this case the maximum of $|\langle m\rangle_{\rm ee}|=BC$ can be achieved in Fig. 1(a) when both B and C are located on the horizontal axis and their distance is maximal (i.e. $\rho=\sigma=0$). Namely, $|\langle m\rangle_{\rm ee}|_{\rm max} = OA+AB+OC$, or equivalently

$$\begin{aligned}|\langle m\rangle_{\rm ee}|_{\rm max} &= m_2\sin^2\theta_{12}\cos^2\theta_{13}\left[1+\sqrt{1-\frac{\Delta m^2_{21}}{m^2_2}}\cot^2\theta_{12}\right.\\ &\quad\left.+\sqrt{1-\frac{\Delta m^2_{21}}{m^2_2}+\frac{\Delta m^2_{31}}{m^2_2}}\frac{\tan^2\theta_{13}}{\sin^2\theta_{12}}\right].\end{aligned} \tag{7}$$

The minimum of $|\langle m\rangle_{\rm ee}|$ is a bit subtle as it must arise from the maximal cancellation among its three complex components [10]. Given $\Delta m^2_{31}>0$, $|\langle m\rangle_{\rm ee}|_{\rm min}=0$ comes out if $\odot O$ and $\odot A$ in Fig. 1 touch or intersect. When $\odot O$ and $\odot A$ are external to each other as shown in Fig. 1(a), $|\langle m\rangle_{\rm ee}|^{\rm (a)}_{\rm min}=OA-AB-OC$, or equivalently

$$\begin{aligned}|\langle m\rangle_{\rm ee}|^{\rm (a)}_{\rm min} &= m_2\sin^2\theta_{12}\cos^2\theta_{13}\left[1-\sqrt{1-\frac{\Delta m^2_{21}}{m^2_2}}\cot^2\theta_{12}\right.\\ &\quad\left.-\sqrt{1-\frac{\Delta m^2_{21}}{m^2_2}+\frac{\Delta m^2_{31}}{m^2_2}}\frac{\tan^2\theta_{13}}{\sin^2\theta_{12}}\right].\end{aligned} \tag{8}$$

But when $\odot O$ is contained in $\odot A$ as shown in Fig. 1(c), $|\langle m\rangle_{\rm ee}|^{\rm (c)}_{\rm min}=AB-OA-OC$; namely,

$$\begin{aligned}|\langle m\rangle_{\rm ee}|^{\rm (c)}_{\rm min} &= m_2\sin^2\theta_{12}\cos^2\theta_{13}\left[\sqrt{1-\frac{\Delta m^2_{21}}{m^2_2}}\cot^2\theta_{12}-1\right.\\ &\quad\left.-\sqrt{1-\frac{\Delta m^2_{21}}{m^2_2}+\frac{\Delta m^2_{31}}{m^2_2}}\frac{\tan^2\theta_{13}}{\sin^2\theta_{12}}\right].\end{aligned} \tag{9}$$

(2) $m_3<m_1<m_2$. In this case $\langle m\rangle_{\rm ee}$ is uniquely described by Fig. 1(c), and its maximum or minimum can be obtained when both B and C are located on the horizontal axis and their distance is maximal (i.e. $\rho=\sigma=0$) or minimal (i.e. $\rho=\pi$ and $\sigma=0$). The expressions of $|\langle m\rangle_{\rm ee}|_{\rm max}$ and $|\langle m\rangle_{\rm ee}|_{\rm min}$ are the same as Eqs. (7) and (9), but the sign of Δm^2_{31} is now negative.

We plot the dependence of $|\langle m\rangle_{\rm ee}|$ on m_2 in Fig. 2 by inputting the 3σ ranges of Δm^2_{21}, Δm^2_{31}, θ_{12} and θ_{13} [8] and allowing the relevant CP-violating phases to vary between 0 and 2π. The numerical results are consistent with the above analytical observation. In particular, the upper or lower bound of $|\langle m\rangle_{\rm ee}|$ in the inverted neutrino mass ordering follows almost the same behavior as that in the normal case, because both of them are governed by Eq. (7) or Eq. (9) with Δm^2_{31} taking the opposite signs. Thanks to $m_2\geqslant\sqrt{\Delta m^2_{21}}$ in the normal case, the allowed region of $|\langle m\rangle_{\rm ee}|$ looks like a hockey stick. But it has to be cut shorter by $|\langle m\rangle_{\rm ee}|<0.19$–$0.45$ eV (or 0.2–0.4 eV) set by the EXO-200 [11] (or GERDA [12]) experiment at the 90% confidence level, and by $m_2<0.08$ eV that is derived from the cosmological constraint $m_1+m_2+m_3<0.23$ eV set by the Planck data [13] at the 95% confidence level.

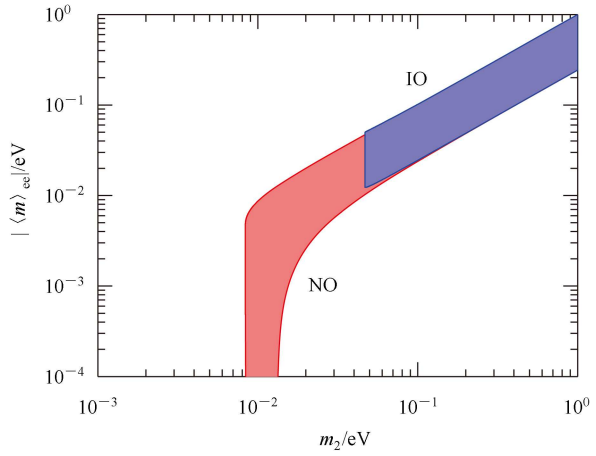

Fig. 2. The dependence of $\langle m\rangle_{\rm ee}$ on m_2 in the normal ordering or inverted ordering of three neutrino masses, where the 3σ ranges of Δm^2_{21}, Δm^2_{31}, θ_{12} and θ_{13} [8] have been input, and the relevant CP-violating phases are allowed to vary between 0 and 2π.

On the other hand, Fig. 2 tells us that $|\langle m\rangle_{\rm ee}|$ tends to approach a very small value and even vanishes when m_2 is not far away from its lower bound $\sqrt{\Delta m^2_{21}}\approx 8.7\times10^{-3}$ eV (i.e. when the base vector $\overrightarrow{OA}$ in Fig. 1 is roughly as short as possible). This observation is certainly true, as geometrically shown in Fig. 1, where a sufficiently short OA means that $\odot O$ and $\odot A$ are more likely to touch or intersect, allowing $|\langle m\rangle_{\rm ee}|\to0$ to naturally take place.

In case the experimental sensitivity has been good enough but a signal of the $0\nu\beta\beta$ decay remains absent, there might be three possibilities: (1) massive neutrinos are the Dirac particles; (2) $|\langle m\rangle_{\rm ee}|$ itself is too small; (3) new physics corrects $\langle m\rangle_{\rm ee}$ in a destructive way to make its size too small. Although $|\langle m\rangle_{\rm ee}|\to0$ implies that it will be impossible to identify the Majorana nature of massive neutrinos via the $0\nu\beta\beta$ decay, this special case is interesting in the sense that it allows us to determine the two Majorana CP-violating phases [9]. As one can see in Fig. 1(b), the quadrilateral becomes a triangle (i.e. $\triangle OP_1A$ or $\triangle OP_2A$) in the $|\langle m\rangle_{\rm ee}|=BC\to0$ limit. Because of $\triangle OP_2A\cong\triangle OP_1A$, we have $\rho=\pi\mp\angle OAP_1$ and $\sigma=\pi\pm\angle AOP_1$ for $\triangle OP_1A$ and $\triangle OP_2A$, respectively. In this case the two inner angles of $\triangle OP_1A$ can be calculated from its three sides OA, $AP_1=AB$ and $OP_1=OC$ by means of the cosine theorem. An analytical discussion has been done in [9] by taking $\langle m\rangle_{\rm ee}=0$ in Eq. (6) to obtain two constraint equations for ρ and σ. From a phenomenological point of view, however, one certainly prefers that the neutrino masses are nearly degenerate or have the inverted ordering, so as to assure $|\langle m\rangle_{\rm ee}|\geqslant10$ MeV which should be accessible in the next-generation $0\nu\beta\beta$ experiments.

Once $|\langle m\rangle_{\rm ee}|$ is determined from a measurement of the CP-conserving $0\nu\beta\beta$ decay, one will be able to partly constrain the absolute neutrino mass scale and two Majorana CP-violating phases [6]. There are two special cases, in which m_2 can be fixed and $\langle m\rangle_{\rm ee}$ only involves a single phase parameter:

(1) $m_1=0$, which leads to $AB=0$. In this case $\odot A$ shrinks into a point, and thus the quadrilateral in Fig. 1 is simplified to $\triangle OAC$. As a result, $|\langle m\rangle_{\rm ee}|$ only depends on a single CP-violating phase:

$$|\langle m\rangle_{\rm ee}|=\sqrt{\Delta m^2_{21}s^4_{12}c^4_{13}+\Delta m^2_{31}s^4_{13}+2\sqrt{\Delta m^2_{21}\Delta m^2_{31}}\,c^2_{12}s^2_{12}s^2_{13}\cos\sigma}. \tag{10}$$

(2) $m_3=0$, which leads to $OC=0$. In this case the quadrilateral in Fig. 1 is simplified to $\triangle OAB$, and the magnitude of $\langle m\rangle_{\rm ee}$ turns out to be

$$|\langle m\rangle_{\rm ee}|=c^2_{13}\sqrt{(\Delta m^2_{21}-\Delta m^2_{31})s^4_{12}-\Delta m^2_{31}c^4_{12}+2\sqrt{\Delta m^2_{31}(\Delta m^2_{31}-\Delta m^2_{21})}\,c^2_{12}s^2_{12}\cos\rho}, \tag{11}$$

which is also dependent upon a single CP-violating phase.

In either case the range of $|\langle m\rangle_{\rm ee}|$ can easily be determined by allowing the respective CP-violating phase to vary from 0 to 2π. With the help of the 3σ ranges of Δm^2_{21}, Δm^2_{31}, θ_{12} and θ_{13} [8], we immediately arrive at 0.68 MeV $\leqslant|\langle m\rangle_{\rm ee}|\leqslant 4.7$ MeV in the $m_1=0$ case, and 12.4 MeV $\leqslant|\langle m\rangle_{\rm ee}|\leqslant 50.1$ MeV in the $m_3=0$ case. The latter is of course more promising in the future $0\nu\beta\beta$ experiments.

3 Comments on $\langle m\rangle_{\alpha\beta}$ and new physics

The coupling-rod diagram of $\langle m\rangle_{\rm ee}$ in Fig. 1 can be extended to geometrically describe $\langle m\rangle_{\alpha\beta}$ (for α, β =e, μ, τ) in general. For each individual $\langle m\rangle_{\alpha\beta}$, it is always possible to adopt a proper parametrization and phase convention of U to make $m_2U_{\alpha2}U_{\beta2}$ real and positive. A typical example of this kind is [14][1)]

$$U=\begin{pmatrix} c'_{12}c'_{13} & s'_{12} & -c'_{12}s'_{13} \\ -c'_{12}s'_{12}c'_{13}+s'_{12}s'_{13}{\rm e}^{-{\rm i}\delta'} & c'_{12}c'_{23} & s'_{12}s'_{13}c'_{23}+c'_{13}s'_{23}{\rm e}^{-{\rm i}\delta'} \\ -s'_{12}c'_{13}s'_{23}-s'_{13}c'_{23}{\rm e}^{-{\rm i}\delta'} & c'_{12}s'_{23} & s'_{12}s'_{13}s'_{23}-c'_{13}c'_{23}{\rm e}^{-{\rm i}\delta'} \end{pmatrix} P'_\nu, \tag{12}$$

where $c'_{ij}\equiv\cos\theta'_{ij}$, $s'_{ij}\equiv\sin\theta'_{ij}$ (for ij=12, 13, 23), and P'_ν is a diagonal matrix containing the other two independent CP-violating phases. Its connection to the standard parametrization of U in Eq. (2) is straightforward. In this case one may express $\langle m\rangle_{\alpha\beta}$ as a sum of three vectors in the complex plane:

$$\langle m\rangle_{\alpha\beta}\equiv\overrightarrow{CB}=\overrightarrow{OA}+\overrightarrow{AB}+\overrightarrow{CO}, \tag{13}$$

where

$$\begin{aligned} \overrightarrow{OA} &\equiv m_2U_{\alpha2}U_{\beta2}=m_2|U_{\alpha2}U_{\beta2}|, \\ \overrightarrow{AB} &\equiv m_1U_{\alpha1}U_{\beta1}=m_1|U_{\alpha1}U_{\beta1}|{\rm e}^{{\rm i}\rho'}, \\ \overrightarrow{CO} &\equiv m_3U_{\alpha3}U_{\beta3}=m_3|U_{\alpha3}U_{\beta3}|{\rm e}^{{\rm i}\sigma'}. \end{aligned} \tag{14}$$

Note that the phase parameters ρ' and σ' depend on the subscripts α and β. Of course, Eq. (13) stands for a quadrilateral which is quite similar to the coupling-rod diagram of $\langle m\rangle_{\rm ee}$ in Fig. 1. Depending on the radii of $\odot O$ and $\odot A$ with respect to $\langle m\rangle_{\alpha\beta}$, Fig. 1(a), (b) and (c) may analogously describe the relative positions of these two circles. An exceptional case, which is not shown in Fig. 1, is that $\odot A$ is likely to be contained in $\odot O$ (i.e., $OC>OA+AB$) for some of the effective Majorana mass terms[2)].

While we do not go into details of the coupling-rod diagrams of $\langle m\rangle_{\alpha\beta}$ in the present work, it is desirable for us to stress the importance of probing these effective neutrino masses in all the possible lepton-number violating processes (e.g. $\langle m\rangle_{\alpha\beta}$ can play an important role in the probabilities of neutrino-antineutrino oscillations and in the rates of $H^{++}\to l^+_\alpha l^+_\beta$ and $H^+\to l_\alpha\overline{\nu}$ decays [15]).

Next, let us briefly comment on possible corrections to $\langle m\rangle_{\alpha\beta}$ from underlying new physics. For simplicity, we assume that the effect of new physics is not correlated with the standard three-flavor $\langle m\rangle_{\alpha\beta}$ in the leading-order approximation but only provides a linear correction to $\langle m\rangle_{\alpha\beta}$ in the form of

$$\langle m\rangle'_{\alpha\beta}=\langle m\rangle_{\alpha\beta}+\text{new physics}. \tag{15}$$

The source of new physics is unknown to us, but some typical examples like the sterile neutrinos and the R-parity violating supersymmetry have been explored in the literature [6]. Because the new-physics term generally involves one or more CP-violating phases, a potential cancellation between it and $\langle m\rangle_{\alpha\beta}$ is likely to lead to vanishing or vanishingly small $\langle m\rangle'_{\alpha\beta}$ [16].

To illustrate, Fig. 3 shows a coupling-rod-like diagram of $\langle m\rangle'_{\rm ee}$ in the presence of new physics described by the $\overrightarrow{BD}$ vector:

$$\langle m\rangle'_{\alpha\beta}\equiv\overrightarrow{CD}=\langle m\rangle_{\alpha\beta}+\overrightarrow{BD}=\overrightarrow{CO}+\overrightarrow{OA}+\overrightarrow{AB}+\overrightarrow{BD}. \tag{16}$$

Depending on the size and phase of $\overrightarrow{BD}$, a number of different configurations of the vectors in Eq. (16) are possible. Fig. 3 only illustrates two simple cases: (a) $\odot O$ and $\odot A$ are external to each other; and (b) $\odot O$ is contained in $\odot A$. Once the nature of new physics is quantitatively fixed, one may give a detailed geometrical description of the salient features of $\langle m\rangle'_{\rm ee}$ as what we have done for $\langle m\rangle_{\rm ee}$ itself.

1) Among the nine possible parametrizations of U listed in [14], patterns (5), (6) and (7) satisfy the requirement because the relevant $U_{\alpha2}$ elements (for $\alpha={\rm e},\mu,\tau$) are all independent of the 'Dirac' CP-violating phase. Hence these elements can also be arranged to be independent of the two Majorana CP-violating phases in a very straightforward way.

2) If the standard parametrization of U in Eq. (2) is applied to Eqs. (13) and (14), a nontrivial issue associated with $\langle m\rangle_{\alpha\beta}$ (for $\alpha\beta\neq$ee) will be that OA and AB become dependent upon the CP-violating phase δ. The latter remains unknown, and thus its uncertainty will more or less complicate our discussions.

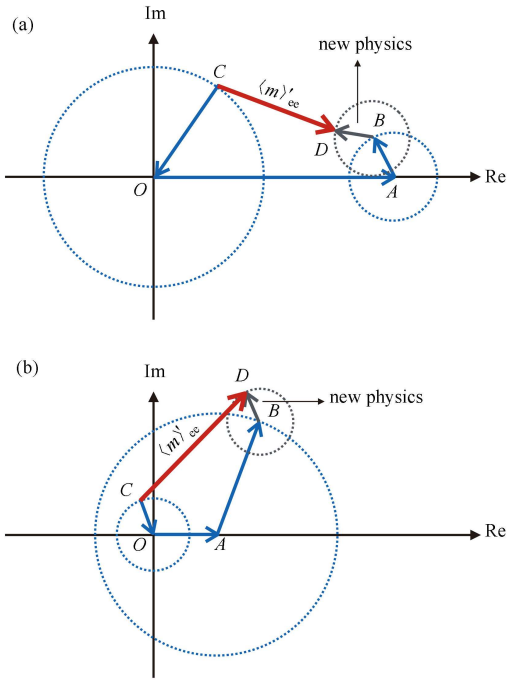

Fig. 3. A coupling-rod-like diagram of $\langle m\rangle'_{ee}\equiv\overrightarrow{CD}$ in the complex plane: (a) $\odot O$ and $\odot A$ are external to each other; and (b) $\odot O$ is contained in $\odot A$, where $\overrightarrow{OA}\equiv m_2|U_{e2}|^2$, $\overrightarrow{AB}\equiv m_1|U_{e1}|^2e^{i\rho}$, $\overrightarrow{CO}\equiv m_3|U_{e3}|^2e^{i\sigma}$, and the new physics contribution is described by the vector $\overrightarrow{BD}$ for illustration.

4 Summary

The $0\nu\beta\beta$ decay has long been recognized as a unique process to identify the Majorana nature of massive neutrinos, and hence searching for its signal becomes almost the most important task in the non-oscillation aspects of today's neutrino physics. Now that the $0\nu\beta\beta$ decay rate depends on the size of the effective Majorana neutrino mass $\langle m\rangle_{ee}$, it is desirable to explore the salient features of $\langle m\rangle_{ee}$ in a phenomenologically favored way. In this work we have put forward a novel coupling-rod diagram to describe $\langle m\rangle_{ee}$ in the complex plane, by which the effects of the neutrino mass ordering and CP-violating phases on $\langle m\rangle_{ee}$ can be intuitively understood. We have shown that this simple geometric language allows us to easily obtain the maximum and minimum of $|\langle m\rangle_{ee}|$. It remains usable even if there is a kind of new physics contributing to $\langle m\rangle_{ee}$. It can also be extended to describe the effective Majorana masses $\langle m\rangle_{e\mu}$, $\langle m\rangle_{e\tau}$, $\langle m\rangle_{\mu\mu}$, $\langle m\rangle_{\mu\tau}$ and $\langle m\rangle_{\tau\tau}$ which may appear in some other lepton-number violating processes, if a proper parametrization and phase convention of the lepton mixing matrix U is adopted.

Although the geometrical and analytical descriptions of $\langle m\rangle_{ee}$ are 'scientifically indistinguishable', 'they are not psychologically identical' in making the underlying physics more transparent [17]. For this reason we expect that the coupling-rod diagram of $\langle m\rangle_{ee}$, just like the unitarity triangles of quark and lepton flavor mixing matrices, can prove to be useful in neutrino phenomenology.

We are indebted to W.L. Guo, Y.F. Li, L.J. Wen and S. Zhou for helpful discussions.

References

1 Majorana E. Nuovo Cimento, 1937, **14**: 171
2 Furry W H. Phys. Rev., 1939, **15**: 1184
3 Bilenky S M, Hosek J, Petcov S T. Phys. Lett. B, 1980, **94**: 495; Schechter J, Valle J W F. Phys. Rev. D, 1980, **22**: 2227; Doi M, Kotani T, Nishiura H, Okuda K, Takasugi E. Phys. Lett. B, 1981, **102**: 323
4 Maki Z, Nakagawa M, Sakata S. Prog. Theor. Phys., 1962, **28**: 870; Pontecorvo B. Sov. Phys. JETP, 1968, **26**: 984
5 Beringer J et al. (Particle Data Group). Phys. Rev. D, 2012, **86**: 010001
6 Rodejohann W. Int. J. Mod. Phys. E, 2011, **20**: 1833
7 Klapdor-Kleingrothaus H V, Päs H, Smirnov A Yu. Phys. Rev. D, 2001, **63**: 073005; Lindner M, Merle A, Rodejohann W. Phys. Rev. D, 2006, **73**: 053005
8 Capozzi F, Fogli G L, Lisi E, Marrone A, Montanino D, Palazzo A. Phys. Rev. D, 2014, **89**: 093018. arXiv:1312.2878
9 XING Z Z. Phys. Rev. D, 2003, **68**: 053002
10 Vissani F. JHEP, 1999, **9906**: 022; Rodejohann W. Nucl. Phys. B, 2001, **597**: 110; Dell'oro S, Marcocci S, Vissani F. Phys. Rev. D, 2014, **90**: 033005. arXiv:1404.2616
11 Albert J B et al. (EXO-200 collaboration). Nature, 2014, **510**: 229–234. arXiv:1402.6956
12 Agostini M et al. (GERDA collaboration). Phys. Rev. Lett., 2013, **111**: 122503
13 Ade P A R et al. (Planck collaboration). Astron. Astrophys. A, 2014, **571**: 16. arXiv:1303.5076
14 Fritzsch H, XING Z Z. Phys. Rev. D, 1998, **57**: 594; XING Z Z. Chin. Phys. C (HEP & NP), 2012, **36**: 281
15 XING Z Z. Phys. Rev. D, 2013, **87**: 053019; XING Z Z, ZHOU Y L. Phys. Rev. D, 2013, **88**: 033002; Merle A, Rodejohann W. Phys. Rev. D, 2006, **73**: 073012
16 LI Y F, LIU S S. Phys. Lett. B, 2012, **706**: 406; XING Z Z. Phys. Rev. D, 2012, **85**: 013008
17 Feynman R P. The Development of the Space Time View of Quantum Electrodynamics (Nobel lecture) reprinted in Physics Today August 1966, 31